

# Numerical and experimental investigation of aerodynamic heat control of leading edge of hypersonic vehicle's flexible skin

Xiaozhou LÜ<sup>1\*</sup>, Chao YUAN<sup>1</sup>, Weimin BAO<sup>2</sup>, Guanghui BAI<sup>2</sup> & Fancheng MENG<sup>3</sup>

<sup>1</sup>*School of Aerospace Science and Technology, Xidian University, Xi'an 710071, China;*

<sup>2</sup>*Science and Technology on Space Physics Laboratory, Beijing 100076, China;*

<sup>3</sup>*College of Materials Science and Engineering, Chongqing University of Technology, Chongqing 400054, China*

Received 23 March 2021/Revised 10 May 2021/Accepted 30 June 2021/Published online 27 September 2022

**Abstract** In this paper, a flexible skin inspired by the sudoriferous gland structure of human skin is developed for ultra-thermal protection of hypersonic morphing vehicles. The effect of different coolants and cooling flow rates on the cooling performance of the leading edge is studied using finite element analysis. A wind tunnel experiment is conducted at high temperatures with the heat flux  $Q = 700 \text{ kW/m}^2$ , and the results indicate the following: (1) the flexible skin can effectively reduce the surface temperature of hypersonic vehicles; (2) when using liquid water instead of argon as the cooling medium, the cooling efficiency of flexible skin performs better; (3) when liquid water is used as the cooling medium, the cooling effect peaks at a flow rate of 0.01 m/s, and further increasing the flow rate will not benefit cooling efficiency significantly; (4) the flexible skin can withstand extreme thermal environments, demonstrating its feasibility in applications of over-limit thermal protection for hypersonic morphing vehicles. This study aims at optimizing the cooling performance of the flexible skin for ultra-thermal protection. The proposed skin can overcome the heat-resistance limit of flexible materials with morphing properties, laying a theoretical and experimental foundation for its future applications in hypersonic morphing vehicles.

**Keywords** hypersonic vehicle, flexible skin, ultra-thermal protection, micro-channel, transpiration cooling

**Citation** Lü X Z, Yuan C, Bao W M, et al. Numerical and experimental investigation of aerodynamic heat control of leading edge of hypersonic vehicle's flexible skin. *Sci China Inf Sci*, 2022, 65(10): 202203, <https://doi.org/10.1007/s11432-021-3312-4>

## 1 Introduction

Hypersonic morphing vehicles [1] are a kind of hypersonic vehicle that can adjust the flight direction and attitude in real-time by changing the tail or wing profiles of the flexible skin. Compared with conventional hypersonic vehicles, hypersonic morphing vehicles can change their fuselage structure to obtain the optimal aerodynamic shape, thereby improving flight efficiency and maneuverability. This allows for hypersonic flight while reducing engine load, fuel consumption, and other flight costs, all of which have a great economic value in various fields such as civilian and military aviation transportation and space transportation [2].

The aerodynamic characteristics of hypersonic vehicles closely correlate with their aerodynamic profile. One of the necessary conditions for realizing the morphing flight of a hypersonic vehicle is that the aerodynamic profile of the vehicle must be a variable. In addition, the vehicle's skin must be resistant to high temperatures. This is because when the vehicle is flying at a speed greater than Mach 5, it produces a strong compression and friction effect on the surrounding air, causing a rapid rise in the surface temperature of the vehicle (referred to as "aerodynamic heat"). As a medium that directly maintains the vehicle's aerodynamic profile, the flexible skin not only guarantees an excellent aerodynamic profile while resisting external pressure but also has outstanding ductility (deformation). Despite these advantages, which can meet the needs of the vehicle for skin deformation, the heat-resisting temperature limitation

\* Corresponding author (email: xzlu@xidian.edu.cn)

of the flexible skin is far lower than that of the vehicle's surface, so the skin cannot withstand extreme thermal environments. Therefore, it is of critical priority to study the transfinite heat-resistant flexible skin for the morphing flight of hypersonic vehicles. A flexible and deformable cross-domain intelligent aircraft is a major change to traditional fixed-profile high-speed vehicles. Due to its continuously variable characteristics, a high-speed vehicle can achieve a variable lift-to-drag ratio, orbital change on demand, and intelligent flight. Consequently, the flexible and deformable cross-domain intelligent vehicle is expected to realize not only continuous morphing according to its task but also intelligent flight according to the environment. The realization of these two functions is a disruptive innovation to the flight mode of traditional fixed-shaped vehicles.

Flexible skins [3] have been used in diverse fields, such as bionic electronics and sensor technology, and have been attracting research interest in the aerospace field. Over the past decades, researchers globally have conducted extensive discussions on flexible skins. In terms of substrate materials used for flexible skins, these studies can be categorized into mechanical deformation, rubber, and shape memory polymer (SMP) substrates as follows.

(a) Flexible skin possessing characteristics of mechanical deformation are made of hard metallic materials, whose bending deformation is realized by special assembly arrangement. In 2002, Rediniotis et al. [4] proposed a metal-based flexible skin with a bionic structure, which is made up of different metallic modules to realize deformation. In 2008, Hutapea et al. [5] fixed a kind of drivable spring on the upper and lower ends of a hypersonic vehicle's wing and realized deformation of the wing by controlling the current.

(b) Flexible skins prepared from rubber used the softness of pure rubber or fiber-reinforced composite rubber to realize deformation. In 2010, Bubert et al. [6] prepared a flexible skin for morphing wings using elastic polymers, which exhibited excellent ductility. In 2016, Jenett et al. [7] proposed an active morphing wing using a crystal-structure flexible polymer, which realized the deformation of the wing by changing the order and geometry of the components [8].

(c) The SMP-based flexible skin is made of smart materials that can remember their shape under the excitation of characteristic physical quantities (such as temperature, electric field, or humidity) to achieve deformation. Bye of Lockheed Martin Airlines [9] used SMP to develop a flexible skin that can change the shape of a flying fuselage and wing from blunt to sharp.

Although the aforementioned types of flexible skins are flexible and morphable to a certain extent, they are only suitable in normal thermal environments (generally  $< 400^{\circ}\text{C}$ ) and can be used merely under low-speed ( $< \text{Mach } 1.2$ ) flight conditions. These flexible materials rarely survive for a long duration when exposed to extreme thermal environments, and they cannot be used under high-speed flight conditions ( $\text{Mach} > 5$ ). Flexible skins that can be used in extreme thermal environments have not been reported so far; however, active thermal protection technology for rigid skins in extreme thermal environments has attracted a lot of attention worldwide.

The active thermal protection mechanism of a rigid skin under an extreme thermal environment mainly includes convection cooling, film cooling, and transpiration cooling, which are, respectively, sketched as follows.

(a) Convection cooling [10] involves regenerative and impingement cooling. In the former, coolants are passed through the cooling channel for convective heat transfer of high-temperature components, whereas the latter is realized by a high-velocity impingement of one or more types of coolants flowing on the surface to dissipate heat. However, convection cooling is frequently used as an auxiliary cooling method due to its low cooling efficiency [11].

(b) Film cooling [12] involves spraying a cooling medium along a heated surface with a certain incident angle, by which a layer of cooling medium film can be attached to the surface, thereby isolating the surface from a high-temperature environment while preventing heat flux erosion. Film cooling demands excessive coolants, exhibiting limitations to some extent.

(c) Transpiration cooling [13] is a cooling method used in porous materials or laminates. The coolant overflows from the heated surface of porous materials, forming a continuous and uniformly distributed membrane structure on the surface, which can isolate a high-temperature environment while preventing heat flux erosion.

Compared with the former two cooling methods, the film formed by transpiration cooling has stronger coverage and a better cooling effect. Owing to its excellent performance, transpiration cooling, which has been widely studied, is regarded as the most promising state-of-the-art technology in future development. In 2009, van Foreest et al. [14] studied the mechanism of using liquid water to realize a vehicle's nose

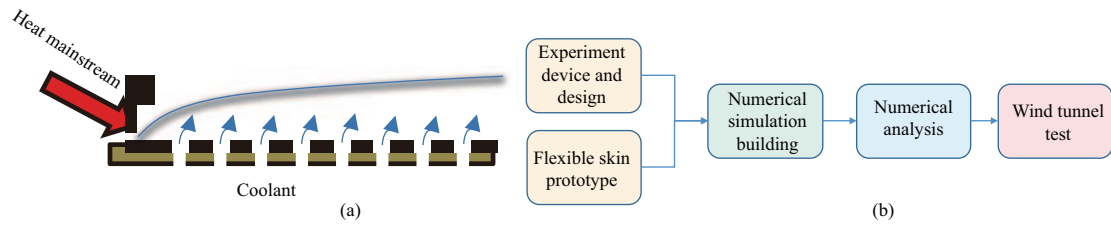


**Figure 1** (Color online) (a) Schematic diagram showing principle of transpiration cooling technology; (b) research flow chart.

cone transpiration cooling and discovered the influences of liquid phase transition and gas film isolation on the vehicle's nose cone cooling effect. In 2019, Wu et al. [15] discussed the effect of gradient porosity distribution on transpiration cooling of the nose cone model. More recently, Huang et al. [16] investigated a thermal protection method that combines transpiration cooling with ablation protection and analyzed the cooling effect of self-pumping structure characterizing with the combination of nickel-based foam and sintered bronze plate.

Although all the above research findings are the thermal protection mechanism of rigid skins (that are mainly made of stainless steel, sintered bronze, carbon, carbon fiber, and other rigid materials) in extreme heat transfer environments and cannot be directly applied to flexible skins, they have guiding and reference significance for flexible skins to overcome the thermal limit.

Considering the aforementioned significance in rigid skin thermal protection, a new concept of flexible skin is, therefore, proposed in this paper, which applies transpiration cooling of active thermal protection technology to flexible skins to provide ultra-thermal protection, overcoming the initial heat-resistance limit of flexible skins while realizing its survival in extreme thermal environments. By simulating the sudoriferous gland structure of human skin, the proposed flexible skin characterized with ultra-thermal protection enables the coolant to pass through interior specific pipes and to form a uniform cooling film over an object surface. Therefore, the ultra-thermal protection ability of flexible skins is realized by combining flexible skin manufacturing technology and transpiration cooling.

The purpose of this work is to develop a flexible skin material for over-limit thermal protection that can withstand high-temperature environments, thereby providing a theoretical and experimental foundation for its application in hypersonic deformable vehicles.

## 2 Numerical simulations and experiments

### 2.1 Experimental device

Transpiration cooling was originally proposed by Hartnett and Eckert and has been proven to be an outstanding cooling method for preventing high-heat-flux components from heat attack. Figure 1(a) shows a transpiration cooling system. When coolant is injected into a porous skin matrix, it can overflow from the intense micro-channel, forming a protective thin film layer covering the heated surface. This process can efficiently reduce the heat impact of the hot mainstream imposed on the surface.

Inspired by the sudoriferous gland structure of human skin, this study designed a bionic transpiration cooling system using flexible skin as porous media. The sudoriferous gland is to secrete perspiration when being excited by an external temperature rise, and the perspiration will evaporate on the surface of the body to dissipate heat.

To simulate this process, we used a flexible skin to simulate human skin. Specifically, a tortuous hollow micro-channel was prepared inside the flexible skin to simulate sudoriferous ducts. The ducts were directly opened on the surface of the flexible skin, and the water outlet, which is referred to as “sudoriferous pore”, was uniformly arranged. A peristaltic pump was used to simulate sudoriferous glands, for which a special cooling medium was used to substitute the perspiration. When the external temperature rises, the peristaltic pump activates, causing the cooling medium to be pumped out and flow along the pipe. Being restricted by the special interior hollow microflow channel, the cooling medium is evenly distributed to each outlet pore to form a uniformly cooling film covering the surface of the flexible skin, thereby conducting further heat exchange between the film and the mainstream.

The tortuous micro-channel was prepared using the lost-wax casting (LWC) method, and a sample of the biomimetic flexible skin is shown in Figure 2. Similarly, the transpiration process also makes the

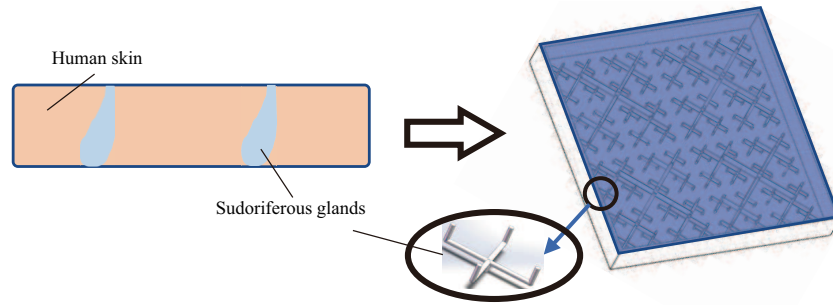


**Figure 2** (Color online) Outside view of the designed flexible skin.

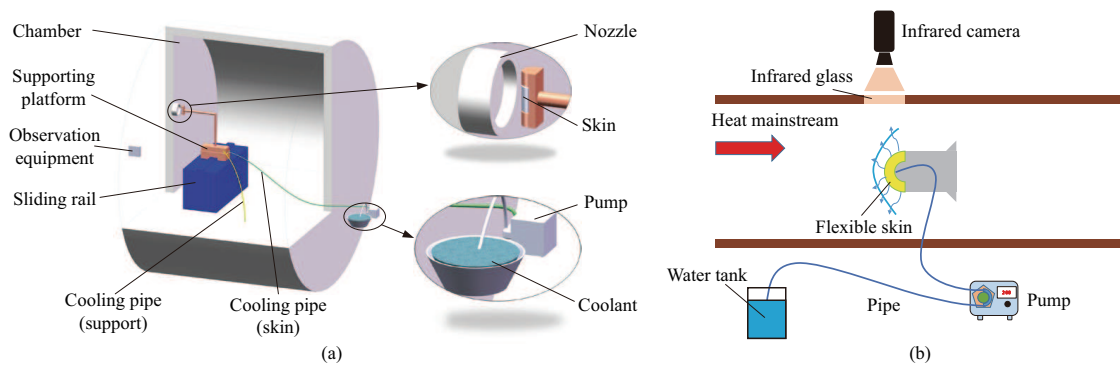


**Figure 3** (Color online) (a) Schematic diagram of experimental equipment; (b) schematic diagram demonstrating the test section.

coolant pass through the interior specific channel, forming a uniform cooling film on the heated surface. In this way, flexible material manufacturing technology and transpiration cooling technology are combined to realize the ultra-thermal protection function of the flexible skin.

Comparing with other parts of hypersonic vehicles, the impact of aerodynamic heat and force exerted on the leading edges is at its peak synchronously near stagnation points, whose amplitudes drastically fluctuate [17–19]. Therefore, designing transpiration cooling on the leading edges of the flexible skin is crucial to broaden the application range of this material. Our study aims to develop the transpiration cooling system on the leading edge bracket and to explore the survival stage of the flexible skin under extreme aerodynamic heat and force.

## 2.2 Preparation of prototype flexible skin

All experiments were conducted in the Key Laboratory of equipment efficiency in an extreme high-temperature environment at the Xidian University of Ministry of Education. Figure 3(a) shows the experimental facility of near-space high-speed plasma. Figure 3(b) shows a schematic diagram of the test section, consisting of a water tank, a pump, a test section, and equipment to measure temperature, pressure, and electrical power input. The equipment used in this study can provide a low-pressure and high-temperature heat stream to realize the simulated flight environment for hypersonic vehicles. First, high-purity argon is delivered into an electric heating section. Then, the hot flow was accelerated to pass through a contraction section and injected onto the surface of the test skin. The hot stream of inlet gas is set with a density  $700 \text{ kW/m}^2$  and pressure of 2 kPa.

By referring to the preparation technology of a micro-fluid chip in the biomedical field [20, 21], the elementary prototype was prepared using the LWC method, which is depicted in Figure 4.

## 2.3 Numerical simulation and boundary conditions

The test section was simplified (as shown in Figure 5(a)) and was modeled using ANSYS ICEM software [22]. Since the supporting platform has been equipped with a water-cooling system whose temperature is not affected by external surroundings, analysis of the supporting platform can be neglected. The established model includes a chamber and skin part (as shown in Figure 5(b)).



Figure 4 (Color online) Physical picture of flexible skin.

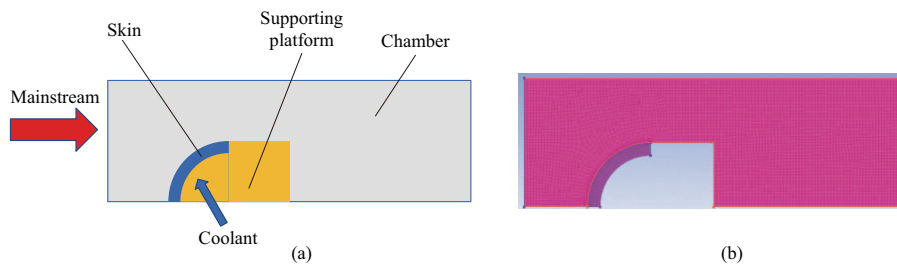


Figure 5 (Color online) Schematic diagram showing. (a) Simulation model and (b) model construction.

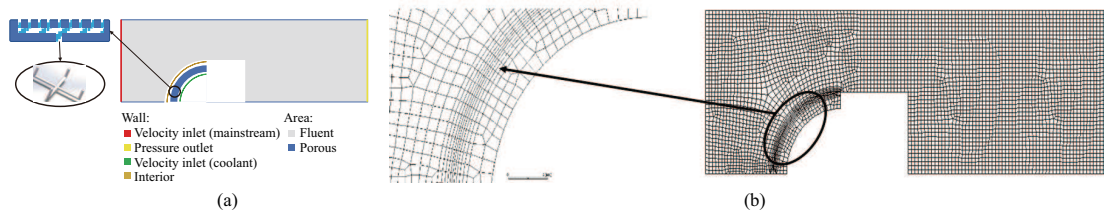


Figure 6 (Color online) (a) Boundary condition setting; (b) dividing the mesh.

The boundary condition setting of finite element analysis is shown in Figure 6(a). When the skin is tortuous, with uncontrollable elastic deformation caused by its interior micro-channels, modeling the actual interior pipes is deemed impractical, and thus, the “porous zone” (located in the corresponding area) is used to replace the actual flexible skin.

Specifically, the corresponding boundary conditions are denoted as follows. Let “velocity inlet” denote the mainstream inlet and “velocity inlet” denote the cooling medium. The flow directions of both the mainstream and cooling medium are perpendicular to the surface. Let “pressure outlet” denote the outlet, “fluid” denote the chamber, and “interior” denote the skin surface. The “Volume of Fluid” model is opened according to the cooling medium selected. The standard “ $k - \varepsilon$ ” model is adopted as the governing equation. Argon is selected as the mainstream. Argon or liquid water is selected as the working cooling medium.

The adaptive meshing function of ICEM is used to divide the target mesh. The meshing results are shown in Figure 6(b). Due to the strong heat exchange phenomenon that occurs on the skin surface, the meshing on the skin surface is subdivided.

The cooling performance of the flexible skin for ultra-thermal protection was evaluated in terms of injection rate  $F = \rho_c V_c / \rho_\infty V_\infty$  [22] and cooling efficiency  $\eta = (T_w - T_\infty) / (T_c - T_\infty)$  [23]. In these two equations,  $\rho_c$  represents the density of the coolant,  $V_c$  represents the velocity of the coolant,  $\rho_\infty$  represents the density of the mainstream,  $V_\infty$  represents the velocity of the mainstream,  $T_w$  represents the external surface temperature of the flexible skin,  $T_c$  represents the temperature of the coolant, and  $T_\infty$  represents the temperature of the mainstream.

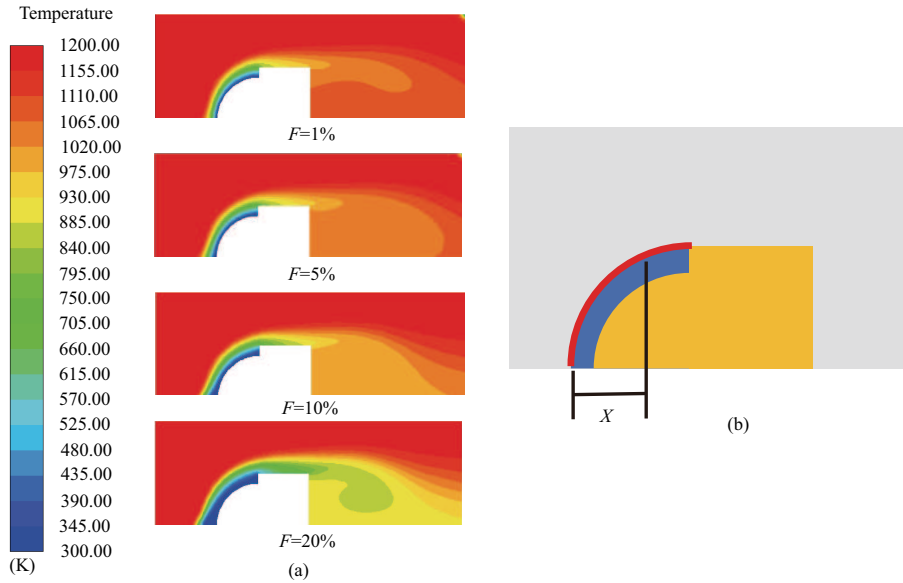


**Figure 7** (Color online) Argon performs as coolant (mainstream temperature is 1200 K and mainstream velocity is 1 m/s). (a) Temperature distribution under different blowing ratios; (b)  $X$ : distance to the stationary point.

### 3 Analysis of simulation and experimental results

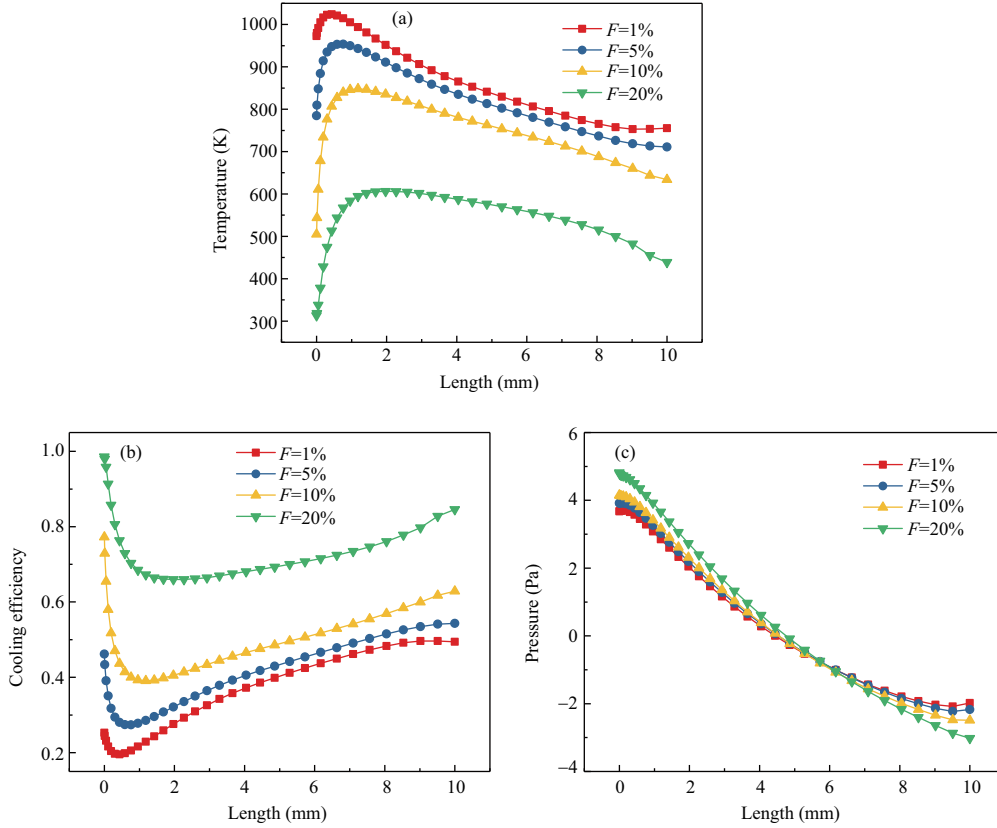
#### 3.1 Cooling efficiency of using argon as coolant

Figure 7 shows the temperature distribution on the skin’s numerical simulation using 300 K argon as the coolant with different blowing ratios of  $F = 1\%$ ,  $F = 5\%$ ,  $F = 10\%$ , and  $F = 20\%$ . The heat stream flows from left to right. The heat stream’s temperature and velocity are 1200 K and 1 m/s, respectively. Figure 7 shows that when the flux of the coolant inlet increases from  $F = 1\%$  to  $F = 20\%$ , significant temperature variation occurs. When the coolant flow rate increases to  $F = 20\%$ , a noticeable color change is observed. In addition, lower temperature areas increase along the  $x$ -axis from the front stagnation point, suggesting that adjusting the injection of the argon coolant is an effective way to reduce the skin temperature of hypersonic vehicles’ leading edges. The temperature of the skin decreases as the flow rate of the coolant increases.

Figure 8 shows the temperature distribution of the external surface, cooling efficiency, and pressure of the flexible skin with different values of  $X$  ranging from 0 to 10. Figure 8(a) shows that when the blowing ratio is 1%, the external surface temperature increases rapidly and then decreases gradually as the distance (the “ $X$ ”) increases. As the coolant flow rate increases, the external surface temperature decreases. For example, when  $F = 20\%$ , the highest temperature (600 K) was 250 K less than that of  $F = 10\%$ , and 550 K less than that of  $F = 1\%$ .

Although the skin temperature at the stagnation point of the leading edge was less than the temperature of other areas, it rapidly increased along the edge and then gradually decreased. At the stagnation point of the leading edge, the direction of the sprayed cooling medium was the opposite of that of the mainstream because the mainstream was isolated by the cooling medium at a far distance and then heat exchange began between them. However, along the external surface of the leading edge, the cooling medium was not directly opposite of the mainstream. The effect of heating and the endothermic process was dominant in this area, and the insulation effect was weakened, resulting in a rapid temperature rise. Subsequently, the front-end cooling medium was enveloped by the mainstream and flown backward, combining both streams at the rear end. When this mixed cooling stream absorbed heat, the angle between the heat stream and the skin gradually reduced, and the intensity of heat exchange intensity weakened, which induced a gradual temperature decrease of the back external surface.

Figure 8(b) shows that when the blowing ratio was 1%, cooling efficiency with respect to the external surface first decreased rapidly and then increased gradually as the distance increased. A larger coolant flow rate implies higher cooling efficiency. For example, when  $F$  was 20% and the distance was 10 mm, the value of cooling efficiency was approximately 0.85. The cooling efficiency of 0.45 was achieved when  $F$  was 1%. When the velocity was  $F = 1\%$  and the distance was 1 mm, cooling efficiency with respect to



**Figure 8** (Color online) Argon performs as coolant under different blowing ratios. (a) Temperature, (b) cooling efficiency, and (c) pressure distributions of the external surface.

the external surface reached the lowest value. In response to different coolant flow rates, the best cooling effect was realized when  $F = 20\%$ . In addition, Figure 8 shows that cooling efficiency increased along the leading edge. Figure 8(c) shows that the pressure of the external surface decreased as the distance increased. Since the tangent direction of the stagnation point of the leading edge was perpendicular to the mainstream, the strongest force of the mainstream occurred at the stagnation point. Due to the low velocity of the heat stream, different flow rates of the coolant had little effect on the pressure distribution of the external surface pressure, resulting in a small pressure gradient around the stagnation point.

Figures 7 and 8 show that using argon as a cooling medium can reduce the external surface temperature of the leading edge and that increasing the argon injection rate can improve cooling efficiency; however, the temperature is still higher than the limiting temperature of the substrate material of the flexible skin. The reasonable explanation for the above situation is that once the low-temperature coolant is sprayed from the flexible skin's external surface, it immediately comes in contact with the mainstream for heat exchange. When the flow rate is small, the cooling medium is instantly heated by the mainstream once it is sprayed out, and its temperature rises rapidly, exceeding the limiting temperature of the flexible skin.

Because the mainstream acts as the sole heating source, improving the injection rate of argon can reduce the external surface temperature of the flexible skin; however, it cannot satisfy the thermal-resistance demand of the flexible skin. Considering practical applications, the heat flux value of the flexible skin exceeds far beyond the simulation value. Therefore, simply increasing the working flow of argon cannot meet the requirement of extreme and harsh thermal protection with respect to hypersonic vehicles, upon which the study of a high-efficient cooling medium has proven to be prioritized.

Transpiration cooling that uses gas as the coolant has been extensively studied [24–27]. To improve transpiration cooling efficiency and the thermal-resistance ability of flexible skins, it is crucial to use certain coolants with high specific heat capacity, among which liquid water is an optimal alternative due to its high specific heat capacity and phase-transition enthalpy. Finite element analysis of the over-limit thermal protection ability of flexible skins using liquid water as a cooling medium is conducted as follows. Since the density of liquid water is significantly higher than that of argon,  $V_c$  is used to replace the  $F$ .

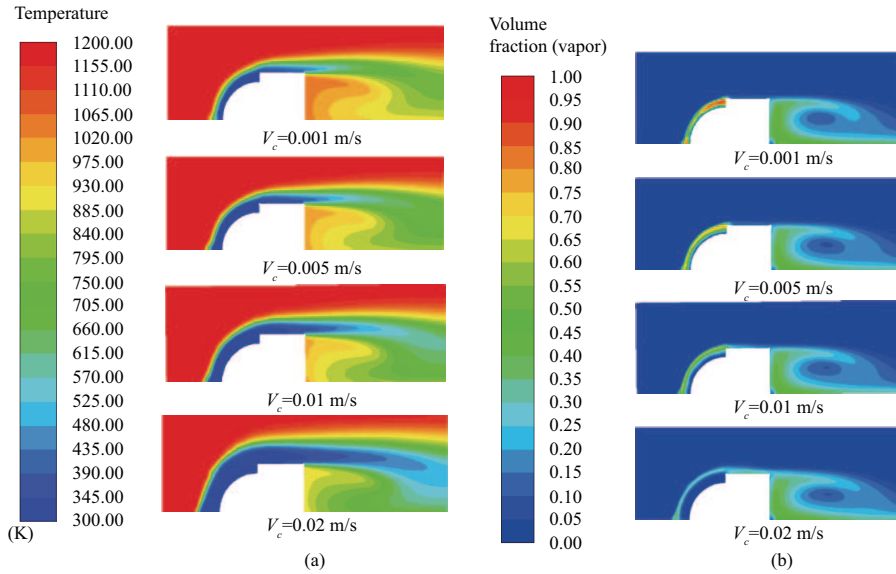


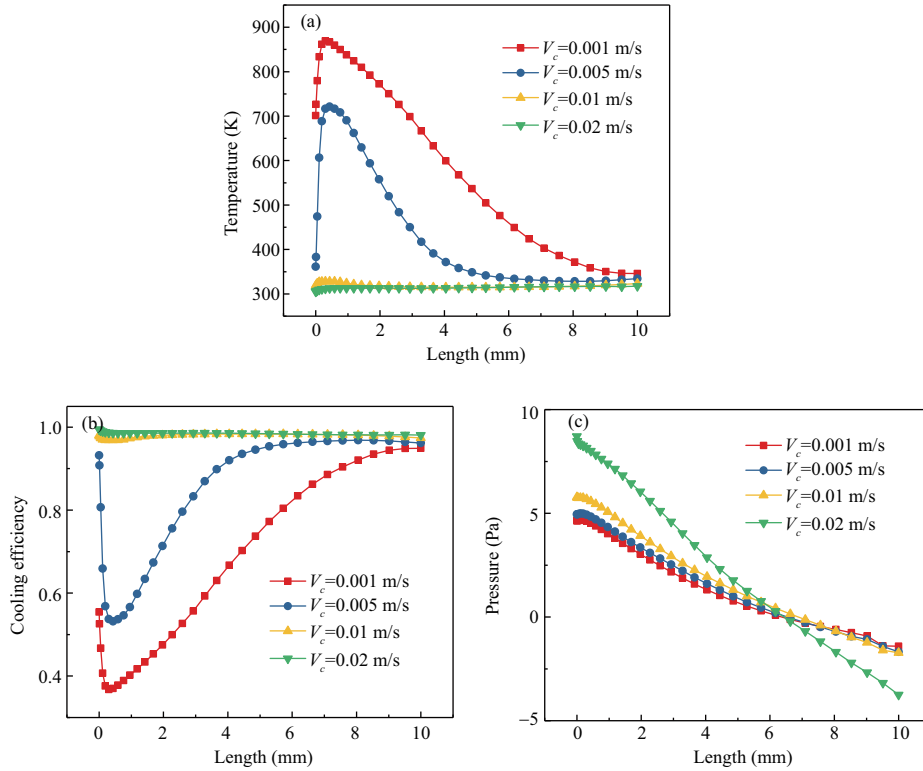
**Figure 9** (Color online) (a) Temperature distribution of liquid water performing as coolant under different blowing ratios; (b) distribution of water vapor volume fraction under different blowing ratios using liquid water as coolant.

### 3.2 Cooling efficiency of liquid water used as coolant

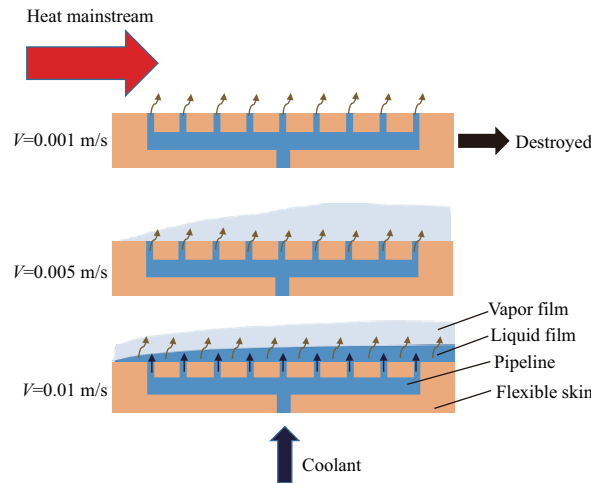
Figure 9(a) shows the nephogram of liquid water's temperature distribution, where the mainstream flow's temperature and velocity are 1200 K and 1 m/s, respectively. The rate of the coolant water flow ranges from 0.001 m/s to 0.02 m/s with a temperature of 300 K, indicating that when the coolant was injected, the color representing the temperature of the flexible skin's external surface changes significantly, suggesting that its external surface temperature is significantly less than the surrounding temperature. As  $V_c$  increases, the low-temperature region on the external surface of the flexible skin gradually diffuses, and the diffusion region is distinct at a coolant flow rate of 0.02 m/s. Furthermore, trailing occurs at the extension line of the leading edge in the low-temperature region; the higher the flow rate, the longer the trailing. This phenomenon implies that the coolant's in-time phase transition does not occur immediately, and excess coolant flows backward under the influence of the mainstream's action. In summary, under the condition of low injection rate, the external surface temperature is higher than the limiting temperature of flexible materials. As the injection rate increases, the external surface temperature decreases rapidly. Under the condition of a high injection rate, the external surface temperature decreases significantly and is lower than the limiting temperature of flexible materials, so that the flexible skin can withstand high-temperature environments. Therefore, using liquid water as a cooling medium can reduce the external surface temperature of the leading edge, with its cooling efficiency significantly outperforming that of high-purity argon.

Figure 9(b) shows the volume fraction distribution nephogram of water vapor at different flow rates of 0.001, 0.005, 0.01, and 0.02 m/s for liquid water. The red region occurs at the far end of the flexible skin when the coolant flows at the rate of 0.001 or 0.005 m/s but vanishes with a further increase in the water flow rate at 0.02 m/s, which indicates that the cooling fluid flows out from the skin's external surface, exchanging heat with the mainstream. After absorbing heat, the temperature of the cooling fluid reaches its boiling point and then undergoes a phase transition to continue absorbing heat. Water vapor will move and gather from the leading edge's front-end to backward-end caused by the action of the mainstream, thereby proving that the occurrences of phase transformation improve heat absorption and realize a transfinite heat protection process.

Figure 10 shows the variation of external surface temperature, cooling efficiency, and pressure of the flexible skin whose length ranges from 0 to 10 under different blowing ratios. Figure 10(a) shows that the trend of temperature variation remains the same when  $V_c$  equals 0.001 and 0.005 m/s. Specifically, the temperature rises rapidly and then decreases gradually as the distance increases. When  $V_c$  exceeds 0.01 m/s, the external surface temperature does not vary significantly, remaining constant at 300 K as the distance increases. In this case, Figure 10(b) shows that cooling efficiency is approximately 100% when  $V_c$  exceeds 0.01 m/s, exhibiting no distinctive variation with the increase in the distance. When  $V_c$  is less



**Figure 10** (Color online) Liquid water performs as coolant under different blowing ratio conditions. (a) External surface temperature distribution; (b) external surface cooling efficiency distribution; (c) external surface pressure distribution.



**Figure 11** (Color online) Outside view of the designed flexible skin.

than 0.01 m/s, cooling efficiency decreases rapidly and then gradually increases as the distance increases, reaching the maximum of approximately 100% at the distance of 10 mm. When  $V_c$  is 0.005 m/s, cooling efficiency (35%) is 20% less than that of  $V_c = 0.05$  m/s. As shown in Figure 10(c), pressure decreases with an increase in distance. When  $V_c$  is 0.02 m/s, pressure reaches the peak value of 9 Pa.

Figure 11 demonstrates the process of liquid water cooling. The over-limit thermal protection process of the flexible skin consists of three parts: heat absorption of the cooling medium heating, heat absorption with phase transition, and thermal insulation from the gas film. The contribution of the three heat-absorption methods will be greatly affected by varying coolant blowing ratios, which can significantly affect the specific contributing percentage of the three heat-absorption methods used throughout the process.

First, when the flow rate of the cooling medium is low (0.001 m/s), the heat emitted from the main-

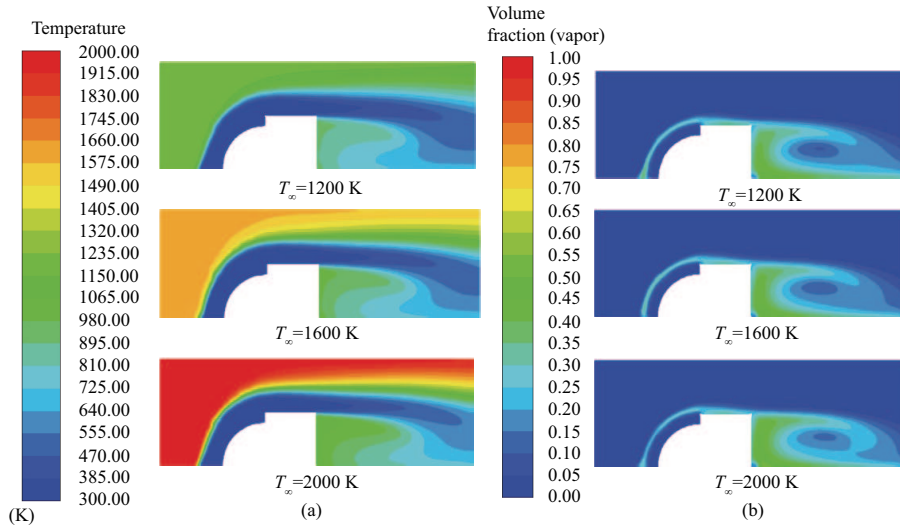


**Figure 12** (Color online) Liquid water performs as coolant (the flow rate is 0.02 m/s, the temperature is 300 K, and the mainstream speed is 1 m/s) under different temperature conditions. (a) Temperature distribution; (b) water vapor volume fraction distribution.

stream is significantly higher than what can be absorbed by the cooling medium heating, making the phase transition in the cooling medium occur rapidly. Nevertheless, the absorbed heat is still significantly less than what is emitted by the mainstream. At this moment, the water phase transition occurs at the skin pipe, whose phase-transition speed far exceeds that of the water flow; therefore, the flexible skin is burned, which is demonstrated in Figures 9(a) and 10(a).

With an increase in the flow rate of the cooling medium (0.005 m/s), the water flows out from the skin's external surface, exchanges heat with the mainstream, and is rapidly heated to absorb heat, during which the water phase transition occurs and heat is dissipated. At this time, the heat absorbed by the outflowing water (i.e., the heat absorbed by the phase transition) equals the heat absorbed by the mainstream, forming water vapor to further prevent the mainstream from being in contact with the skin. Under this circumstance, the speed of water phase transition is the same as that of the outflowing water, and the entire process consists of rising water temperatures, heat absorption, phase transition, and gas film insulation.

Further increasing the flow rate of water to 0.01 m/s, the speed of water phase transition becomes slower than that of the outflowing water, resulting in excess water forming a layer of water film on the skin's external surface to isolate the mainstream and moving backward under the action of the mainstream, which explains the trailing of the low-temperature region at the leading edge's extension line in Figure 9. Increasing the flow rate of water to 0.02 m/s has no discernible effect on cooling efficiency. Therefore, Figures 7, 8(b), 9, and 10(b) show that although the injection amount of the liquid cooling medium is less than that of the gas cooling medium, the former's cooling effect outperforms that of the latter. Our future study will focus on the flexible skin with ultra-thermal protection and liquid water performing as a cooling medium.

Figure 12 shows the temperature distribution and water vapor volume fraction distribution nephogram of the numerical simulation for liquid water, where the temperature and velocity of the coolant water are 300 K and 0.02 m/s, respectively. The mainstream temperature ranges from 1200 to 2000 K, and the flow rate is 1 m/s.

Figure 12(a) shows that with an increase in distance, three situations are presented as follows. (1) The temperature color changes from green to blue when the mainstream temperature is 1200 K; (2) the color changes from yellow to blue when the mainstream temperature is 1600 K; (3) the color changes from red to blue when the mainstream temperature is 2000 K. Among these three mainstream temperatures, the most significant color change occurs at 2000 K. In addition, Figure 12(b) shows that when the temperature rises, the volume fraction distribution of water vapor exhibits insignificant changes, suggesting that the influence of temperature imposed on the cooling effect of the skin can be neglected and that the flexible skin can withstand a high mainstream temperature of 2000 K.

Figure 13 shows the temperature, variation of cooling efficiency, and pressure distribution of the flexible skin's external surface with respect to the distance. Figure 13(a) shows that when the mainstream

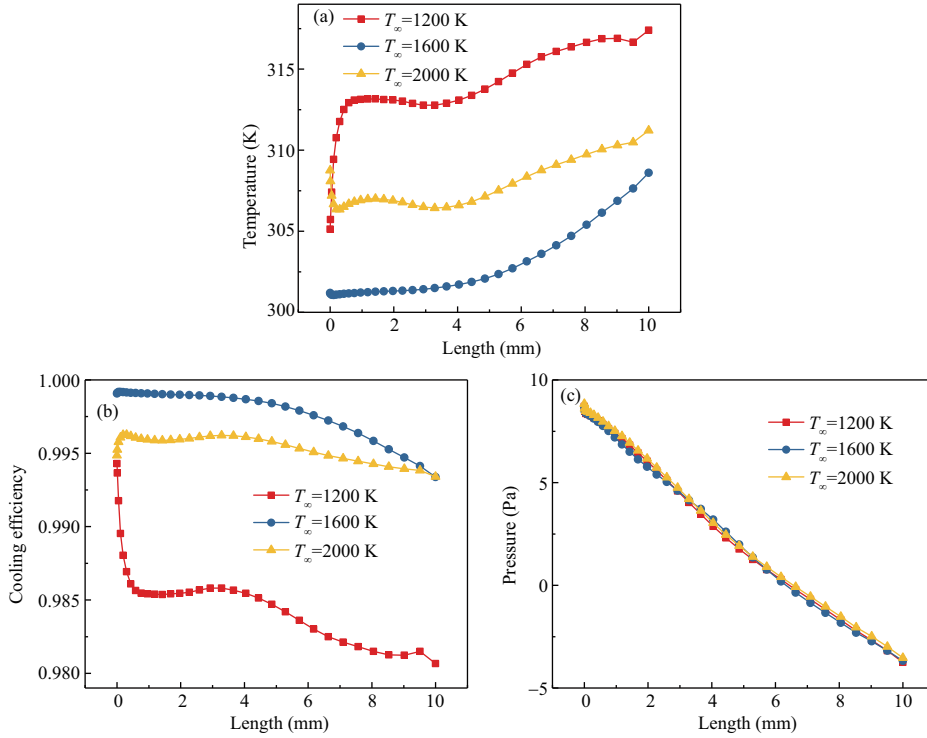


**Figure 13** (Color online) Liquid water performs as coolant (speed is 0.02 m/s, temperature is 300 K, and the mainstream speed is 1 m/s) under different temperature conditions. (a) External surface temperature distribution; (b) cooling efficiency distribution; (c) pressure distribution.

temperature is 1200 K, the external surface temperature first increases rapidly as the distance increases, then slowly decreases, and gradually rises; Figure 13(b) shows that when the mainstream temperature is 1600 K, the external surface temperature increases continuously as the distance increases; Figure 13(c) shows that when the mainstream temperature is 2000 K, the external surface temperature first decreases with an increase in distance and then increases with a small fluctuation. The external surface temperature of the flexible skin remains at its lowest value when the mainstream temperature is 1600 K. All external surface temperatures are invariably lower than the limiting temperature of the flexible material. Therefore, it is believed that even at the mainstream temperature of 2000 K, the limiting temperature of the over-limit thermal protection flexible skin is not reached.

Figure 13(b) shows that (1) when the mainstream temperature is 1200 K, the external surface cooling efficiency first decreases with an increase in distance and then remains constant. As the distance exceeds 5 mm, cooling efficiency begins to decrease gradually. The variation trend at 1600 K is similar to that at 2000 K, suggesting that cooling efficiency at both temperatures decreases with an increase in distance. (2) When the mainstream temperature is 1600 K, the external surface cooling efficiency of the flexible skin remains at its highest value. As the distance increases, cooling efficiency first decreases and then fluctuates slightly, after which it gradually decreases. Figure 13(c) shows that the three different curves of external surface pressure almost overlap with each other at the three mainstream temperatures, all of which decrease with an increase in distance, suggesting that the temperature significantly affects the pressure.

### 3.3 Ground wind tunnel experiment

Using water as the coolant and considering all simulation results, the performance of the over-limit thermal protection flexible skin is studied, where the heat stream inlet has a density of 700 kW/m<sup>2</sup>, a pressure of 2 kPa, and the coolant flow rate and temperature are 0.005 m/s and 300 K, respectively.

When the coolant flow rate is 0.005 m/s, the external surface of the flexible skin is burned during the experiment, but the region near the interior pipe is unburned, as shown in Figure 14. Two reasonable explanations can be attributed to the above situation. One explanation is that ablation happens on the skin's external surface due to the nonexistence of coolant before coolant injection. The other explanation



**Figure 14** (Color online) Burn-out of flexible skin.

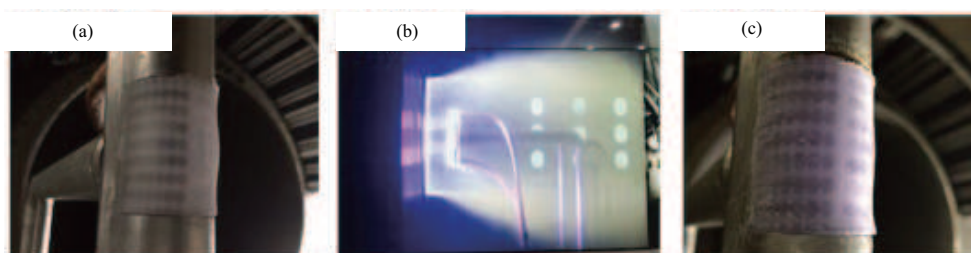


**Figure 15** (Color online) Comparison of flexible skin before and after the experiment. (a) Before testing; (b) testing; (c) after testing.

is that ablation occurs after the coolant injection since the coolant being injected is insufficient to support the flexible skin to withstand the heat flow.

In response to the failed result in Figure 14, an innovative experiment was conducted during which the mode of skin motion and the amount of coolant injection were optimized. First, only after the flexible skin's external surface is stably covered with the coolant can the skin be placed to be in contact with the mainstream. Second, improving the coolant's injection rate is another crucial factor affecting the experimental results. The second experiment shown in Figure 15 was a success, where the flexible skin withstood an extreme thermal environment, validating the feasibility of the flexible skin characterized with over-limit thermal protection.

The ultimate temperature of the flexible skin is significantly lower than that of the mainstream. According to the experimental results, no damage has been found on the surface of the flexible skin, indicating that the flexible skin is not in direct contact with the mainstream. The cooling liquid flows out from the surface of the flexible skin under the restriction of the internal micro-channels of the flexible skin, forming a cooling film to completely cover the flexible skin. The cooling film prevents the flexible skin from being in direct contact with the mainstream. In this experiment, liquid water was used as the cooling medium. Both the specific heat capacity and the latent heat of vaporization of water are high. The water film formed during the experiment can absorb a large amount of heat.

During the experiment, liquid water was sprayed out from the surface of the skin to form a uniform water film covering the skin's surface. The water film isolated the skin from the mainstream, thereby preventing the skin from directly participating in the heat exchange process. The water film exchanged heat with the mainstream, during which the liquid water was heated, absorbing part of the heat. Then, the temperature reached the phase change point, and the phase change of the liquid water absorbed part of the heat. Due to the high specific heat capacity and latent heat of vaporization of liquid water, the formed water film can effectively reduce the skin's surface temperature. In addition, water vapor generated by the vaporized water formed a layer of gas film on the skin's surface, strengthening the heat insulation effect of the gas film. In addition, the water film always underwent a repeated cycle of replenishment, consumption, and loss during the experiment. The cooling film can be considered dynamic, which demands fewer requirements for the cooling film's thermal protection capability and is easier to achieve. The successful front-edge ground wind tunnel experiment revealed that the flexible skin meets both high-temperature resistance and morphing characteristics. The corresponding detailed experimental research will be presented in our future work.

The flexible skin prepared in this paper is of great significance to the development of high-speed de-

formable vehicles. On the one hand, flexible skin can be directly used in high-speed morphing aircraft. The skin can withstand the extreme thermal environment of the surface of high-speed aircraft, overcoming the restriction of the “aerodynamic heat effect” occurring on the traditional flexible skin. On the other hand, the principle of the skin has reference significance for future research concerning the skin of hypersonic deformable aircraft. Regardless of whether the aircraft’s skin can withstand extreme heat, the effective cooling film on the surface of the aircraft insulates the skin from heat exchange with the air [28].

## 4 Conclusion

By combining the finite element analysis (simulation) results with experimental verification results, we have proposed a flexible skin inspired by the sudoriferous gland structure of human skin, which is characterized with ultra-thermal protection, for hypersonic morphing vehicles. In this study, we designed a biomimetic transpiration cooling system using the proposed flexible skin as porous media. According to the simulation and experimental results, our research findings are formulated as follows.

The as-prepared flexible skin can effectively reduce the external surface temperature of hypersonic vehicles, exhibiting excellent performance in extremely harsh environments. In addition, owing to the specific heat capacity of liquid water, which is significantly higher than that of argon, the liquid water’s cooling effect greatly outperforms that of argon. When liquid water is used as the cooling medium, the flexible skin characterized with ultra-thermal protection can withstand an extreme temperature of 2000 K with the maximum cooling fluid flow rate of 0.01 m/s. Further, increasing the coolant flow rate will not significantly improve cooling efficiency. The cooling process consists of three parts: temperature rising, phase transition, and film insulation. The limiting temperature for the survival of the flexible skin needs to be further explored.

The flexible skin characterized with ultra-thermal protection passed the ground wind tunnel test. The experimental results suggest that the flexible skin can withstand an extreme thermal temperature of up to 1200 s (700 kW/m<sup>2</sup>), overcoming the thermal-resistance limit of flexible materials while providing a theoretical and experimental foundation for expanding the application range of flexible skins in hypersonic vehicles.

**Acknowledgements** This work was supported by the Open Foundation of the Key Laboratory of Equipment Efficiency in Extreme Environments, Ministry of Education of China.

## References

- 1 Bao C, Wang P, Tang G. Integrated method of guidance, control and morphing for hypersonic morphing vehicle in glide phase. *Chin J Aeronaut*, 2021, 34: 535–553
- 2 Tsien H S. Similarity laws of hypersonic flows. *J Math Phys*, 2012, 25: 247–251
- 3 Guo Q, He X, Wang Z, et al. Effects of wing flexibility on aerodynamic performance of an aircraft model. *Chin J Aeronaut*, 2021, 34: 133–142
- 4 Rediniotis O K, Wilson L N, Lagoudas D C, et al. Development of a shape-memory-alloy actuated biomimetic hydrofoil. *J Intell Material Syst Struct*, 2002, 13: 35–49
- 5 Hutapea P, Kim J, Guion A, et al. Development of a smart wing. *Aircraft Eng Aerospace Tech*, 2008, 80: 439–444
- 6 Bubert E A, Woods B K S, Lee K, et al. Design and fabrication of a passive 1D morphing aircraft skin. *J Intell Material Syst Struct*, 2010, 21: 1699–1717
- 7 Jenett B, Calisch S, Cellucci D, et al. Digital morphing wing: active wing shaping concept using composite lattice-based cellular structures. *Soft Robot*, 2017, 4: 33–48
- 8 Yazik M H, Sultan M T H, Shah A U M, et al. Effect of MWCNT content on thermal and shape memory properties of epoxy nanocomposites as material for morphing wing skin. *J Therm Anal Calorim*, 2020, 139: 147–158
- 9 Bye D, McClure P. Design of a morphing vehicle. In: *Proceedings of the 48th AIAA/ASME/ASCE/AHS/ASC Structures, Structural Dynamics, and Materials Conference*, 2007
- 10 Cheng T, Li W, Lu W, et al. Heat transfer and failure mode analyses of ultrahigh-temperature ceramic thermal protection system of hypersonic vehicles. *Math Problems Eng*, 2014, 2014: 1–11
- 11 Fereidooni A, Marchwica J, Leung N, et al. Development of a hybrid (rigid-flexible) morphing leading edge equipped with bending and extending capabilities. *J Intell Mater Syst Struct*, 2021, 32: 1024–1037
- 12 Kim S M, Lee K D, Kim K Y. A comparative analysis of various shaped film-cooling holes. *Heat Mass Transfer*, 2012, 48: 1929–1939
- 13 Bhushan B. Bioinspired structured surfaces. *Langmuir*, 2012, 28: 1698–1714
- 14 van Foreest A, Sippel M, Gülhan A, et al. Transpiration cooling using liquid water. *J Therm Heat Transf*, 2009, 23: 693–702

- 15 Wu N, Wang J, He F, et al. An experimental investigation on transpiration cooling of a nose cone model with a gradient porosity layout. *Exp Thermal Fluid Sci*, 2019, 106: 194–201
- 16 Huang G, Liao Z, Xu R, et al. Self-pumping transpiration cooling with a protective porous armor. *Appl Thermal Eng*, 2020, 164: 114485
- 17 Anderson J D. *Hypersonic and High Temperature Gas Dynamics*. New York: Mc Graw Hill Book Company, 1998. 288–295
- 18 Ding R, Wang J, He F, et al. Numerical investigation on a double layer combined cooling structure for aerodynamic heat control of hypersonic vehicle leading edge. *Appl Thermal Eng*, 2020, 169: 114949
- 19 Liu Y Q, Jiang P X, Jin S S, et al. Transpiration cooling of a nose cone by various foreign gases. *Int J Heat Mass Transfer*, 2010, 53: 5364–5372
- 20 Sackmann E K, Fulton A L, Beebe D J. The present and future role of microfluidics in biomedical research. *Nature*, 2014, 507: 181–189
- 21 Whitesides G M. The origins and the future of microfluidics. *Nature*, 2006, 442: 368–373
- 22 Huang G, Zhu Y H, Liao Z Y, et al. Transpiration cooling with bio-inspired structured surfaces. *Bioinspir Biomim*, 2020, 15: 036016
- 23 Langener T, von Wolfersdorf J, Selzer M, et al. Experimental investigations of transpiration cooling applied to C/C material. *Int J Thermal Sci*, 2012, 54: 70–81
- 24 Kuhn M, Hald H, Gülhan A, et al. Experimental investigations of transpiration cooled CMC's in supersonic plasma flows. In: *Proceedings of European Workshop on Thermal Protection Systems and Hot Structures Conference*, 2006
- 25 Bellettre J, Bataille F, Lallemand A, et al. Studies of the transpiration cooling through a sintered stainless steel plate. *Exp Heat Transfer*, 2005, 18: 33–44
- 26 Bellettre J, Bataille F, Lallemand A. Prediction of thermal protection of walls by blowing with different fluids. *Int J Thermal Sci*, 1999, 38: 492–500
- 27 Lezuo M, Haidn O J. Transpiration cooling using gaseous hydrogen. In: *Proceedings of the 33rd Joint Propulsion Conference and Exhibit*, Seattle, 1997
- 28 Zhang S, Li X, Zuo J, et al. Research progress on active thermal protection for hypersonic vehicles. *Prog Aerospace Sci*, 2020, 119: 100646